Structural Characterization of Nickel−Doped Aluminum Oxide Cations by Cryogenic Ion Trap Vibrational Spectroscopy

Yake Li,[1,2,#] Mark C. Babin,[3,#] Sreekanta Debnath,[1,2] Takeshi Iwasa,[4] Sonu Kumar,[5] Tetsuya Taketsugu,[4,5] Knut Asmis[,1], Andrey Lyalin,*[,5,6] Daniel M. Neumark*[,3,7]*

[1] Wilhelm−Ostwald−Institut für Physikalische und Theoretische Chemie, Universität Leipzig, Linnéstrasse 2, 04103 Leipzig, Germany

[2] Fritz−Haber−Institut der Max−Plank−Gesellschaft, Faradayweg 4−6, 14195 Berlin, Germany

[3] Department of Chemistry, University of California, Berkeley, California 94720, United States

[4] Department of Chemistry, Faculty of Science, Hokkaido University, Sapporo 060−0810, Japan

[5] Institute for Chemical Reaction Design and Discovery (WPI−ICReDD), Hokkaido University, Sapporo, 001−0021, Japan

[6] Center for Green Research on Energy and Environmental Materials, National Institute for Material Science (NIMS), Tsukuba 305−0044, Japan

[7] Chemical Sciences Division, Lawrence Berkeley National Laboratory, Berkeley, California 94720, United States

[#] Contributed equally to this work

*Correspondence to: knut.asmis@uni−lepzig.de, dneumark@berkeley.edu, lyalin@icredd.hokudai.ac.jp

Abstract

Nickel-doped aluminum oxide cations $(NiO_m)(Al_2O_3)_n(AlO)^+$ with m = 1−2 and n = 1−3 are investigated by infrared photodissociation (IRPD) spectroscopy in combination with density functional theory and the single component artificial force induced reaction method. IRPD spectra of the corresponding He-tagged cations are reported in the 400−1200 cm^{-1} spectral range and assigned based on a comparison to calculated harmonic IR spectra of low energy isomers. Simulated spectra of the lowest energy structures generally match the experimental spectra, but multiple isomers may contribute to the spectra of the m = 2 series. The identified structures of the oxides (m = 1) correspond to inserting a Ni-O moiety into an Al-O bond of the corresponding $(Al_2O_3)_{1\text{-}3}(AlO)^+$ cluster, yielding either a doubly or triply-coordinated Ni^{2+} center. The m = 2 clusters prefer similar structures in which the additional O-atom is either incorporated into a peroxide unit, leaving the oxidation state of the Ni^{2+} atom unchanged, or forms a biradical comprising a terminal oxygen radical anion $Al{-}O^{\bullet-}$ and a Ni^{3+} species. These clusters represent model systems for under coordinated Ni-sites in alumina-supported Ni catalysts and should prove helpful in disentangling the mechanism of selective oxidative dehydrogenation of alkanes by Ni-doped catalysts.

Introduction

Alumina−supported nickel−based catalysts, Ni/Al_2O_3, constitute an important class of catalytic materials with a wide range of industrial applications, such as natural gas reforming for syngas production[1-2] and oxidative dehydrogenation (ODH) of alkanes.[3-4] When used in ODH catalysis, it has been assumed that the active species in these materials are NiO crystallites dispersed on alumina and nickel aluminate species ($NiAl_2O_4$), both with Ni in its common +2 oxidation state. These morphologies believed to be responsible for the high selectivity of this class of catalyst as compared to unsupported pure NiO crystallites. However, more recently, the formation of Ni^{3+} species, which promote the isolation of electrophilic oxygen (O^-), has been invoked to explain the high selectivity for ethylene formation from ethane.[3] The complexity and inhomogeneity of the condensed phase reaction environment often precludes a complete molecular−level understanding of the active species and underlying reaction mechanisms. Therefore, it proves helpful to study small metal oxide clusters in the gas phase. Such clusters provide atom−specific insights into the interactions governing structures−reactivity correlations at the molecular level and ultimately can serve as isolated model systems for active sites in real catalysts.[5-9]

Here, we study the geometric and electronic structure of $Ni_xAl_yO_z^+$ clusters in order to identify such model systems for Ni/Al_2O_3 ODH catalysts. As charged clusters are required for mass selection, we have chosen mixed metal oxide cations with the composition $(NiO_m)(Al_2O_3)_n(AlO)^+$ with m = 1−2 and n = 1−3. For m = 1, the addition of the NiO moiety ensures formally fully oxidized clusters with all metal atoms in their most common oxidation state (Al^{3+} and Ni^{2+}). Addition of one more O atom in the m = 2 series allows for the study of oxygen-rich species, which may contain less common Ni^{3+} centres in combination with O^- species such as those invoked to explain enhanced ODH selectivity.

There exists a substantial body of work exploring the gas phase spectroscopy of aluminium oxide clusters.[10-24] Aluminium oxide anions have been investigated by UV photoelectron,[10-16] IR matrix−isolation[19] and IR resonance−enhanced multiphoton ionization spectroscopy.[18] Detailed structural information has also been obtained by infrared photodissociation (IRPD) spectroscopy of messenger−tagged anionic and cationic clusters.[20-24] These studies show that the $(Al_2O_3)_{1-4}(AlO)^+$ and $(Al_2O_3)_{1-6}AlO_2^-$ series indeed form electronically closed−shell structures composed exclusively of Al^{3+} and O^{2-}.[21, 24] The preferred geometric structures are rather irregular and typically require a genetic algorithm for identification.[20] The corresponding IR spectra are complex and start to converge to that of amorphous alumina for systems containing more than ~25 atoms.[24] Less is known concerning the spectroscopy of metal−doped aluminium clusters, which can represent challenging benchmarks even for advanced electronic structure methods.[25-26] Ni−doped aluminium oxide clusters have not been studied previously by theory or experiment.

In the following, we characterize the Ni−containing aluminum oxide cations $(NiO_m)(Al_2O_3)_n(AlO)^+$ with m = 1−2 and n = 1−3 using cryogenic ion trap vibrational spectroscopy.[27-28] IRPD spectra of the He−tagged cations are compared to predicted spectra from density function theory (DFT). Cluster structures are optimized using the automated reaction path search technique by the artificial force induced reaction method (AFIR),[29-31] allowing for a systematic search for molecular or cluster structures and chemical reaction pathways. We show that unambiguous structural assignments are possible based on a comparison to the spectra of low energy isomers. We then discuss the geometric and electronic nature of the Ni−site and identify clusters that may be particularly useful as model systems in future reactivity studies.

Experimental Methods

The infrared photodissociation (IRPD) experiments were performed using a cryogenic ion trap tandem mass spectrometer[32-33] interfaced with widely tunable, intense IR radiation from the Fritz−Haber−Institute Free−Electron Laser (FHI FEL).[34] In brief, $Ni_xAl_yO_z^+$ cluster cations were prepared by laser ablation of a mixed Ni/Al rod (Ni:Al = 1:1 molar ratio) in the presence of 1 % O_2 seeded in 6 atm He carrier gas. The subsequent beam of cations passes through a 4 mm diameter skimmer and is collimated in a radio frequency (RF) decapole ion guide. The desired cations are mass−selected using a quadrupole mass filter, deflected 90° by an electrostatic quadrupole deflector, and focused into a cryogenic RF ring−electrode ion trap. The trap is continuously filled with He buffer gas at an ion−trap temperature of 10 K. In the trap, the cations are accumulated, thermalized, and messenger−tagged through collisions with the buffer gas, forming $(NiO_m)(Al_2O_3)_n(AlO)^+ \cdot He_x$ (x = 1−3) complexes.

For IRPD experiments, all ions are extracted from the trap at 5 Hz and focused both temporally and spatially into the center of the extraction region of an orthogonally mounted reflection time−of−flight (TOF) tandem photofragmentation mass−spectrometer. Here, the ions are irradiated with a counter−propagating IR laser pulse produced by the FHI FEL (400−1200 cm^{-1}, bandwidth: ~0.5 % FWHM, pulse energy: 0.2−5 mJ). All parent and photofragment ions are then accelerated toward an MCP detector and monitored simultaneously. IRPD scans are recorded by averaging about 100 TOF mass spectra per wavelength step (3 cm^{-1}) and scanning the wavelength. Typically, at least three scans are averaged to obtain the final IRPD spectrum. The photodissociation cross section σ_{IRPD} is determined as described previously.[35-36]

Computational Methods

Initial screening of geometry structures of $(NiO_m)(Al_2O_3)_n(AlO)^+$ with m = 1−2 and n = 1−3 clusters was performed using the single−component artificial force induced reaction (SC−AFIR)

method,[29-31] implemented in the GRRM17 package.[37-38] This method has been successfully used in our previous work for a systematic investigation of the optimized geometries, structural fluxionality and pathways of chemical reactions catalyzed by atomic clusters.[39-41] The collision energy parameter γ of the AFIR method was set to 100 kJ/mol. In the structural searches, DFT computations were performed with TURBOMOLE[42-43] using the def−SV(P) basis sets [44] with the BP86 functional[45-46] under the resolution of identity approximation.[47]

The obtained geometries are further refined using the Becke three−parameter exchange and Lee–Yang–Parr correlation functional (B3LYP)[48-49] and the def2−TZVP basis set[50-51] as implemented in the Gaussian 16 program package.[52] Harmonic vibrational frequencies and IR intensities are determined at the B3LYP/def2−TZVP optimized geometries. All energies reported are zero−point energy (ZPE) corrected with the unscaled frequencies. Simulated spectra are derived from the B3LYP/def2−TZVP scaled harmonic frequencies and intensities and convoluted with a 15 cm^{-1} fwhm Gaussian line shape function to account for rotational band contours as well as the spectral width of the laser pulse. Best agreement is found for a scaling factor of 1.011.

To obtain a quantitative measure for the agreement of experimental and theoretical spectra, the cosine similarity score is used.[53] The score S expresses the similarity between two spectra, where the intensity of the experimental and predicted absorptions is represented by vectors A and B in eq. (1). The score can vary from zero to unity, with a value closer to 1 indicating greater similarity.

$$S = \cos(\theta) = \frac{A \cdot B}{\|A\|\|B\|} = \frac{\sum_{i=1}^{n} A_i B_i}{\sqrt{\sum_{i=1}^{n} A_i^2}\ \sqrt{\sum_{i=1}^{n} B_i^2}} \qquad (1)$$

All systems studied here contain a Ni atom with a partially filled d shell and hence states of different multiplicity need to be considered with the high spin configurations typically yielding

the most reliable single determinant wavefunction. For Ni^{2+} (d^8 configuration), this corresponds to the triplet state manifold and we therefore focus our discussion on these triplet states and their structures, energies and harmonic IR spectra. The corresponding open-shell singlet wavefunctions typically yield very similar, quasi iso-energetic structures with similar IR spectra (see Figure S3). For the systems containing a terminal oxygen radical anion (**D−1** and **E−1** in Figure 3) the situation is more complex. Formally, these systems contain (up to) four unpaired electrons, three electrons delocalized over a $Ni(-O-)_3$ moiety, either in a high-spin (quartet) or low-spin (doublet) configuration, weakly coupled to the electron centered on the terminal oxygen atom. This yields states of either quintet, triplet or singlet multiplicity. However, the $Ni(-O-)_3$ high-spin solutions are found at higher energy than the low-spin ones. Therefore the results for the triplet states containing the Ni low-spin configuration (**D−1** and **E−1**) are shown. Note that also here the structures and spectra for the different multiplicities are very similar (see Figs. S3-5). Finally, it should be noted that D_1 diagnostics (matrix 2-norm of coupled cluster amplitudes for single excitations) performed with the use of TURBOMOLE package demonstrates that the wavefunction of structures **D−1** and **E−1** possess essentially multi-configuration character due to the presence of degenerate and quasi-degenerate states.[54] Therefore, an improved description of the corresponding wavefunctions requires the use of the multireference ab initio theory such as CASPT2[55] and MRCI,[56] which goes far beyond the scope of the present study.

Results and Discussion

<Figure 1 >

A representative mass spectrum of the metal oxide cations produced by laser ablation of an Al/Ni rod is shown in Figure 1. The pure aluminum oxide cations $(Al_2O_3)_n(AlO)^+$ with $n = 1−3$

are among the most abundantly formed ions. Their exceptional stability has been noted previously[21] and is a reflection of their closed electron shell combined with all atoms nominally being in their favored oxidation state, i.e. Al^{3+} and O^{2-}. Addition of $Ni^{2+}O^{2-}$ to this series yields the mixed metal oxides $(NiO)(Al_2O_3)_n(AlO)^+$ with $n = 1-3$, which are among the most prominent Ni−containing clusters in the mass spectrum, in line with the assumption that the most stable clusters contain the elements in their preferred oxidation state. Analysis of the relative mass peak intensities of the cations containing a single Ni atom reveals intensity patterns that reflect the natural isotope distribution of Ni, suggesting that the contribution of clusters with different stoichiometry but identical mass−to−charge ratio is small. (see inset in Figure 1).

<Figure 2 >

IRPD spectra of the $(NiO_m)(Al_2O_3)_n(AlO)^+$ with $m = 1-2$ and $n = 1-3$ are shown in Figure 2. No absorption is observed above 1100 cm^{-1}. The most intense IR signals are found at the highest wavenumbers, i.e. in the 900−1100 cm^{-1} spectral range, with the spectra of the $m = 2$ series (oxygen-rich) either exhibiting strong IR absorptions substantially blue−shifted ($n = 1, 2$) or at similar positions ($n = 3$) to those of the corresponding features in the spectra of the $m = 1$ series (oxides). The spectrum of the largest cluster ($n = 3$) in both series exhibits the largest number of bands and substantial IR activity is observed down to 600 cm^{-1}, suggesting the formation of irregular “amorphous−like” structures, as was reported previously for larger aluminum oxide anions.[24]

<Figure 3 >

In order to assign structures to the experimentally obtained IRPD spectra, we performed electronic structure calculations using DFT. We chose the SC−AFIR approach[29-31] as part of a global reaction route mapping (GRRM) strategy,[37-38] as a similar approach has been successfully

used in our previous work.[39-41] The geometries of low−energy structural candidates were then optimized using B3LYP/def2−tzvp. For each cluster size, three low−energy isomers are shown in Figure 3. In some cases, we find nearly isoenergetic isomers with similar structures and IR spectra, in which case we chose to display the next lowest isomer that exhibits a different structure. The formal oxidation state of the Ni atom is assigned based on an analysis of the spin densities and coordination numbers (see Fig. S2). Relative coordination numbers and other geometric parameters are listed in Table 1.

In general, we find that formation of four- (4m) and six-membered (6m) rings is preferred by the atoms comprising the aluminum oxide framework. We also find that the average O and Al coordination numbers are in the range 2.0−2.5 and 3.0−3.6, respectively, which are substantially smaller than the corresponding values of 4 and 6 in bulk α-alumina. The values for the gas phase clusters are closer to those reported for amorphous alumina as well as thin films (see Table 1), while the Ni atom is either doubly or triply coordinated. Moreover, all oxide clusters (m = 1) shown in Fig. 3 exclusively contain Ni^{2+} centers, while the oxide-rich clusters (m = 2) either contain a peroxo-unit in combination with a Ni^{2+} center or form a structure with a Ni^{3+} species on one side of the cluster and a terminal oxygen radical anion $Al{-}O^{\bullet-}$ on the other.

<Table 1 >

<Figure 4 >

The experimental IRPD spectra of He−tagged $(NiO)(Al_2O_3)_n(AlO)^+$ cations with n = 1−3 are compared to the computed spectra of the corresponding low−energy isomers (see Figure 3) in Figure 4. Table S1 in the SI summarizes the experimental band positions, computed scaled frequencies and band assignments.

For n = 1, the lowest energy isomer (**A−1**) has C_s symmetry. It comprises two edge-sharing 4m rings as part of a Al_3O_3 book-like moiety and a 6m ring including the doubly coordinated Ni^{2+} atom, which lies in the symmetry plane (Ni−O bond length: 180 pm). **A−2** is found 106 kJ/mol higher in energy. It comprises two 6m rings and one 4m ring, with the Ni forming a short and a long Ni−O bond (176/191 pm). **A−3** (+137 kJ / mol) is the most disordered structure and also has a doubly coordinated Ni^{2+} in a locally asymmetric environment.

The simulated spectrum of the lowest energy isomer **A−1** exhibits the highest cosine similarity score (0.88) and is much higher than that of the spectra of the other two isomers **A−2** (0.03) and **A−3** (0.62). We therefore assign the symmetric structure **A−1** to the $(NiO)(Al_2O_3)(AlO)^+$ cation. The highest energy band at 978 cm^{-1} results from excitation of the symmetric combination of the two symmetry-equivalent antisymmetric $O^2{-}Al^3{-}O^2$ stretching modes (see Figure S6). The other IR−active bands are mainly due to the stretching or bending modes involving the two edge-sharing 4m rings (700−900 cm^{-1}) and the stretching or bending modes of the O−Ni−O moiety (450−650 cm^{-1}).

The lowest energy isomer for n = 2 is the quasi−planar C_1 structure **B−1.** Its Al−O framework shows similarities with **A−1** in so far as it also contains the Al_3O_3 book-like motif as well as a doubly coordinated Ni^{2+} atom as part of a 6m−ring, but with slightly shorter Ni−O bond lengths (179/178 pm). **B−2** is slightly higher in energy (+4 kJ / mol). It is a cage−like, more symmetric structure (C_s), consisting of one 4m and two 6m AlO rings, as well as an 8m ring with a symmetric O−Ni−O moiety. The higher energy isomer **B−3** (+31 kJ / mol) is again a sheet like structure with similarities to **B−1**, such as the Al_3O_3 book motif and a 6m ring containing the doubly coordinated Ni^{2+} center.

The simulated spectrum of the lowest energy isomer **B−1** exhibits the highest similarity score (0.88) of the three isomers. It reproduces the experimental spectrum satisfactorily, while the spectra of **B−2** (0.78) and **B−3** (0.41) predict bands with substantial IR activity below 1000 cm^{-1} that are not observed. We therefore assign structure **B−1** to the $(NiO)(Al_2O_3)_2(AlO)^+$ cation. The highest energy band at 1044 cm^{-1} (b_1) can be assigned to a mode that is similar to the one described for **A-1** involving a combination of two antisymmetric $O^2{-}Al^3{-}O^2$ stretching modes joined by the Ni^{2+} atom (see Fig. S6).

The lowest energy isomer for n = 3 (**C−1)** is a three-dimensional structure of C_1 symmetry and the first to contain two four-fold coordinated Al^{3+} sites together with a triply-coordinated Ni^{2+} atom. It consists of five 6m and three 4m fused rings. These form a cone-like structure with a rim consisting of a characteristic 10m AlO ring, quite similar to that reported for $(Al_2O_3)_3(AlO)^+$.[21] The higher energy isomers **C−2** (+83 kJ / mol) and **C−3** (+86 kJ / mol) only exhibit a single four-fold coordinated Al^{3+} atom and adopt more quasi-planar structures.

The simulated spectrum of the lowest energy isomer (**C−1**) again exhibits a significantly higher cosine similarity score (0.90) than the spectra of the other two isomers **C−2** (0.41) and **C−3** (0.47). We therefore assign the cone-like structure **C−1** to the $(NiO)(Al_2O_3)_3(AlO)^+$ cation. The two highest energy bands c_1 (1035 cm^{-1}) and c_2 (993 cm^{-1}) are assigned to antisymmetric −O−(Al)−O− stretches within the 10m ring (see Fig. S6). Note that these vibrational frequencies are similar to the highest energy rim modes (1029 cm^{-1}) reported previously for the pure aluminum oxide cation $(Al_2O_3)_3(AlO)^+$ lending further support to this assignment.[21]

Collectively, the structures found for the oxide series $(NiO)(Al_2O_3)_{1\text{-}3}(AlO)$ correspond to insertion of a Ni-O moiety into an Al-O bond of the previously reported lowest energy $(Al_2O_3)_{1\text{-}3}AlO^+$ isomers for all three sizes.[21] Moreover, nickel is formally always present as Ni^{2+}

in a d^8 configuration and either doubly (n = 1, 2) or triply coordinated (n = 3). Here, we have focussed on Ni in its high spin d^8 configuration (triplet state). The corresponding singlet states (low spin d^8 configuration) are found to be nearly isoenergetic and with similar IR spectra (see SI). The most intense IR features are found at the highest wavenumbers, namely at 978 cm^{-1} (n = 1), 1044 cm^{-1} (n = 2), and 1035 cm^{-1} (n = 3). They involve excitation of particularly short Al-O bonds (168−174 pm, see Table S2) as part of a combination of O^2−Al^3−O^2 antisymmetric stretching modes. This matches well with results reported previously on aluminum oxide anions, where frequencies in this spectral range 900 − 1050 cm^{-1} were reported for similar modes.[24] The IR intensities of the bands associated with Ni−O modes (n = 1: $a_{6,7}$; n = 2: $b_{10,11}$; n = 3: $c_{10,13,14}$), on the other hand, are rather small.

Experimental IRPD spectra of the oxygen-rich $(NiO_2)(Al_2O_3)_n(AlO)^+$ cations with n = 1−3 are compared to the computed spectra of the corresponding low−energy isomers (see Figure 3) in Figure 5. Experimental band positions, computed scaled frequencies and band assignments can be found in Table S1.

<Figure 5 >

The lowest energy isomer predicted for n = 1 is the quasi-planar C_s structure **D−1**. Its structure is similar to that of **A−1**, but the positions of the Ni- and the Al-atom in the symmetry plane are switched and the extra O-atom is added such that metal centers are now triply coordinated. In comparison to the m = 1 structures, **D−1** includes a triply coordinated Ni-site and a terminal oxygen−centered radical anion (Al−$O^{\bullet-}$) on the opposite side of the cation. Analysis of the spin densities, including spin polarization effects, suggests the presence of a Ni^{3+} species, where the spin is delocalized over the Ni(-O-)$_3$ moiety, either in a high-spin (quartet) or low-spin (doublet) configuration. The additional unpaired electron centered on the terminal oxygen atom can then be

coupled in either a parallel or antiparallel fashion yielding states of quintet, triplet or singlet multiplicity. For simplicity, we focus on the triplet states here, but note that the IR spectra of the corresponding quintet state (see Figs. S4) is very similar. Of the two possible triplets, **D-1** corresponds to the one with the low-spin configration on the Ni(-O-)$_3$ moiety and a parallel spin on the terminal oxygen atom. The higher energy isomers **D−2** (+14 kJ/mol) and **D−3** (+18 kJ/mol) are variants of structure **A−1**, in which the Ni-atom remains in its original position in the form of a doubly−coordinated Ni^{2+} center. The additional O-atom is incorporated in the form of an O_2^{2-} unit, between either Ni/Al or Al/Al sites and with a bond length (155 pm) that is typical for peroxo species.[23]

The simulated spectrum of the lowest energy isomer **D−1** exhibits the highest cosine similarity of these three isomers, but its magnitude (0.65) is considerably smaller than the scores found for the best matches for the m = 1 series (≥ 0.88). Three bands (d_{2-4}) observed in the experiment are not reproduced by the simulated spectrum and two bands are predicted around 700 cm^{-1}, which are not observed experimentally. Despite these discrepancies, the spectrum of **D−1** is the best match and we assign the structure accordingly. The spectrum of the higher energy isomer **D−2** (0.40) reproduces the unassigned bands d_{2-4} and therefore is probably present in the experiment, but with lower abundance than **D−1**. The assignment of the highest energy band d_1 (1053 cm^{-1}) is similar to that of band a_1 in the spectrum of **A-1** (see Fig. S6). The band corresponding to the Al−$O^{\bullet-}$ stretching mode is predicted at 906 cm^{-1} with low IR-intensity and is tentatively assigned to the feature at 912 cm^{-1} in the experimental IRPD spectrum.

For n = 2, the situation is quite similar to that for n = 1. The lowest energy isomer **E−1** can be derived from the corresponding m = 1 structure **B−1**. Similar to **D−1**, **E−1** includes a triply coordinated Ni^{3+} site in combination with a terminal oxygen radical at the opposite end of the

cation. The cage−like structure **E−2**, which contains two 4-fold coordinated Al^{3+} sites, is predicted +33 kJ/mol higher in energy and includes a triply coordinated Ni^{2+} site with three spins located on the NiO_2 moiety forming two Ni-O bonds (186/187 pm). The higher energy isomer **E−3** (+38 kJ/mol) is similar to **E−1** in that it is quasi-planar and contains a triply-coordinated Ni^{3+} site. Interestingly, it does not exhibit a terminal O radical with a localized spin, but rather the spin is now delocalized over the two O atoms of the 4m Al_2O_2 ring. The distance between these two oxygen atoms is 224 pm, much larger than that for a typical superoxo unit (~132 pm).[23]

The cosine similarity score of the **E−1** spectrum (0.76) is considerably higher than those of **E−2** (0.42) and **E−3** spectrum (0.46) and we assign the structure of the $(NiO_2)(Al_2O_3)_2(AlO)^+$ cation accordingly. However, smaller contributions to the experimental IRPD spectrum from other isomers, specifically **E−2**, are likely. The assignment of the highest energy band e_1 (1084 cm^{-1}) is the same as for **D−1** and involves the two O^2−Al^3−O^2 moieties adjacent to the terminal Al−$O^{\bullet-}$ unit. Band e_4 (933 cm^{-1}) is then tentatively assigned to the Al−$O^{\bullet-}$ stretching mode (see Table 2).

For n = 3, all three low−energy isomers exhibit three−dimensional structures containing exclusively triply−coordinated Ni^{2+} centers. All three structures represent variations of the corresponding m = 1 cone-like structure **C−1.** They only differ in the location of the peroxo-group, which is found adjacent to the Ni atom in **F−1** and further away as part of the rim structure in **F−2** (+21 kJ / mol) and **F−3** (+34 kJ / mol).

This is the only system for which the spectrum of the lowest energy isomer does not yield the highest cosine similarity score. The score for the spectrum of **F−1** (0.73) is smaller than the corresponding value for the spectrum for **F−2** (0.86). Indeed, it seems likely that both isomers contribute to the experimental spectrum with **F−2** being the main contributor. While the spectrum of **F−2** reproduces nearly all features at lower energies, only the spectrum of **F−1** can account for

the highest energy peak i_1 (1039 cm^{-1}). The spectrum of **F−3** exhibits the lowest similarity score (0.53) of the three isomers. Bands f_1 and f_2 are attributed to the same mode as already described for **C−1** (see Fig. S6). The peroxo stretching modes are predicted at 911 cm^{-1}(**F−1**) and 864 cm^{-1} (**F−2**) with low IR intensity and in a congested spectral range, making their identification challenging.

Altogether, the structures identified for the m = 2 (oxygen-rich) series $(NiO_2)(Al_2O_3)_{1\text{-}3}(AlO)^+$ are related to the structures found for the m = 1 (oxide) series in that they exhibit a similar framework. In contrast to the m = 1 cations, however, multiple isomers probably contribute to the spectra of the m = 2 cations, probably due to the lower relative stability of the latter (see also Figure 1). Further, we find that the additional O-atom can be incorporated in two ways. For n = 2, we find the Ni^{3+}/Al-$O^{\bullet-}$ motif, while the most stable structures for n = 3 prefer the Ni^{2+}/O_2^{2-} motif. Both structural motifs are found to contribute to the experimental spectrum for n = 1. With increasing cluster size, the number of fourfold- (and higher-fold) coordinated Al-atoms increases and three-dimensional (3D) structures are preferred and these stabilize the Ni^{2+}/O_2^{2-} motif. Note that the chemical reactivity is expected to be different for the two types of oxygen species (O_2^{2-} vs. Al−$O^{\bullet-}$). Al−$O^{\bullet-}$ groups are typically more reactive and the ability of terminal oxygen radicals to activate methane is well documented.[57]

For the moderate cluster sizes (n = 3) characterized here, we find that cone-like 3D structures, originally identified for the corresponding $(Al_2O_3)_{1-4}(AlO)^+$ cations[21] are particularly stable. While the most intense IR bands in these spectra are due to combinations of O^2−Al^3−O^2 antisymmetric stretching modes involving particularly short Al−O bonds (< 173 pm), the modes involving the characteristic oxygen species (either O_2^{2-} or Al−$O^{\bullet-}$) as well as the Ni-O modes are predicted too low in IR intensity to be observed unambiguously experimentally.

DFT does a surprisingly good job for these challenging systems, which really should be treated with multi-reference approaches. Even though the DFT energies are not predictive for transition metal containing systems as studied here,[26] the lowest energy isomer is typically (but not always) found to be the structure that contributes predominantly to the IRPD spectrum. For most systems, we find satisfactory agreement with the spectra of clusters containing the Ni atom in a high spin configuration. However, since the predicted spectra for the corresponding systems with lower multiplicity are typically very similar, we cannot infer reliably on their spin state. This would require the application of other techniques, like x-ray magnetic circular dichroism spectroscopy.[58]

Conclusion

Vibrational spectra of nickel-doped aluminum oxide cations, $(NiO_m)(Al_2O_3)_n(AlO)^+$ m = 1–2, n = 1–3 have been obtained using IRPD spectroscopy of He-tagged ions. These spectra show a wealth of vibrational structure in the 400-1200 cm^{-1} spectral range and assignments are facilitated through comparison with computed harmonic IR spectra of low energy isomers. For m = 1, we find satisfactory agreement with the spectra of clusters that show the insertion of a Ni–O moiety into an Al–O bond of the corresponding $(Al_2O_3)_{1\text{-}3}(AlO)^+$ cations, resulting in doubly and triply-coordinated Ni^{2+} centers. The oxigen-rich cations $(NiO_2)(Al_2O_3)_{1\text{-}3}(AlO)^+$ contain either a $Ni^{3+}/Al\text{-}O^{\bullet-}$ or a Ni^{2+}/O_2^{2-} motif and represent gas phase model systems for undercoordinated alumina-supported Ni-sites in oxygen-rich environments. Further reactivity studies on these model systems have the potential to unravel the mechanism of the industrially-relevant ODH of alkanes by alumina−supported nickel−based catalysts, in particular, the origin of the observed high selectivity.

ASSOCIATED CONTENT

Supporting Information.

Comparison between experimental and harmonic IR spectra, experimental band positions, harmonic ferquencies and band assignments, bond length ranges as a function of coordination number, spin density distributions for the lowest energy isomers, comparison of harmonic IR spectra of states with similar structure but different multiplicity, schematic representation of the normal modes with highest IR activity.

AUTHOR INFORMATION

Corresponding Author

*Email: knut.asmis@uni−lepzig.de, dneumark@berkeley.edu, lyalin.andrey@nims.go.jp.

ORCID

Ya-Ke Li: 0000-0003-1877-1922

Mark C. Babin: 0000-0001-7440-8058

Sreekanta Debnath: 0000-0001-9585-1876

Takeshi Iwasa: 0000-0002-1611-7380

Sonu Kumar: 0000-0002-3807-836X

Tetsuya Taketsugu: 0000-0002-1337-6694

Knut Asmis: 0000-0001-6297-5856

Andrey Lyalin: 0000-0001-6589-0006

Daniel M. Neumark: 0000-0002-3762-9473

Notes

The authors declare no competing financial interests.

Acknowledgements

Ya−Ke Li thanks the Alexander−von−Humboldt Foundation for a post−doctoral research fellowship. Mark C. Babin thanks the Army Research Office for a National Defense Science and Engineering Graduate fellowship. This work has been funded by Deutsche Forschungsgemeinschaft (DFG, German Research Foundation) within project 430942176 (Asmis). DMN and MCB acknowledge support from the Air Force Office of Scientific Research under Grant No. FA9550-19-1-0051. Calculations were partially performed using computational resources of the Numerical Materials Simulator, NIMS, Tsukuba, Japan, and the MASAMUNE−IMR supercomputer at the Center for Computational Materials Science, Institute for Materials Research, Tohoku University (Project No. K2101). Institute for Chemical Reaction Design and Discovery (ICReDD) was established by World Premier International Research Initiative (WPI), MEXT, Japan. This work was also partly supported by the Japan Society for the Promotion of Science (JSPS) KAKENHI (Grant No. JP20K05592), Elements Strategy Initiative of MEXT (Grant No. JPMXP0112101003), the Photoexcitonix Project at Hokkaido University, and JST CREST, Japan (Grant No. JPMJCR1902).

References

1. Alvarez-Galvan, C.; Melian, M.; Ruiz-Matas, L.; Eslava, J. L.; Navarro, R. M.; Ahmadi, M.; Cuenya, B. R.; Fierro, J. L. G., Partial Oxidation of Methane to Syngas Over Nickel-Based Catalysts: Influence of Support Type, Addition of Rhodium, and Preparation Method. *Front. Chem.* **2019,** *7*, 1-16.
2. Aramouni, N. A. K.; Touma, J. G.; Tarboush, B. A.; Zeaiter, J.; Ahmad, M. N., Catalyst Design for Dry Reforming of Methane: Analysis Review. *Renew. Sust. Energ. Rev.* **2018,** *82*, 2570-2585.
3. Zhou, Y.; Wei, F.; Lin, J.; Li, L.; Li, X.; Qi, H.; Pan, X.; Liu, X.; Huang, C.; Lin, S.; Wang, X., Sulfate-Modified NiAl Mixed Oxides as Effective C–H Bond-Breaking Agents for the Sole Production of Ethylene from Ethane. *ACS Catal.* **2020,** *10*, 7619-7629.
4. Heracleous, E.; Lee, A.; Wilson, K.; Lemonidou, A., Investigation of Ni-based Alumina-Supported Catalysts for the Oxidative Dehydrogenation of Ethane to Ethylene: Structural Characterization and Reactivity Studies. *J. Catal.* **2005,** *231*, 159-171.
5. Böhme, D. K.; Schwarz, H., Gas-Phase Catalysis by Atomic and Cluster Metal Ions: The Ultimate Single-Site Catalysts. *Angew. Chem. Int. Ed.* **2005,** *44*, 2336 – 2354.
6. Castleman, A. W., Cluster Structure and Reactions: Gaining Insights into Catalytic Processes. *Catal. Lett.* **2011,** *141*, 1243–1253.
7. Sauer, J.; Freund, H.-J., Models in Catalysis. *Catal. Lett.* **2015,** *145*, 109-125.
8. Andris, E.; Navrátil, R.; Jašík, J.; Terencio, T.; Srnec, M.; Costas, M.; Roithová, J., Chasing the Evasive Fe=O Stretch and the Spin State of the Iron(IV)–Oxo Complexes by Photodissociation Spectroscopy. *J. Am. Chem. Soc.* **2017,** *139*, 2757-2765.

9. Schwarz, H.; Asmis, K. R., Identification of Active Sites and Structural Characterization of Reactive Ionic Intermediates by Cryogenic Ion Trap Vibrational Spectroscopy. *Chem. Eur. J.* **2019,** *25*, 2112-2126.

10. Desai, S. R.; Wu, H. B.; Wang, L. S., Vibrationally Resolved Photoelectron Spectroscopy of AlO^- and AlO_2. *Int. J. Mass Spectrom. Ion Process.* **1996,** *159*, 75-80.

11. Desai, S. R.; Wu, H.; Rohlfing, C. M.; Wang, L.-S., A Study of the Structure and Bonding of Small Aluminum Oxide Clusters by Photoelectron Spectroscopy: $Al_xO_y^-$ (x = 1–2, y = 1–5). *J. Chem. Phys.* **1997,** *106*, 1309-1317.

12. Wu, H. B.; Li, X.; Wang, X. B.; Ding, C. F.; Wang, L. S., Al_3O_y (y = 0-5) Clusters: Sequential Oxidation, Metal-to-Oxide Transformation, and Photoisomerization. *J. Chem. Phys.* **1998,** *109*, 449-458.

13. Akin, F. A.; Jarrold, C. C., Addition of Water and Methanol to $Al_3O_3^-$ Studied by Mass Spectrometry and Anion Photoelectron Spectroscopy. *J. Chem. Phys.* **2003,** *118*, 5841-5851.

14. Das, U.; Raghavachari, K.; Jarrold, C. C., Addition of Water to $Al_5O_4^-$ Determined by Anion Photoelectron Spectroscopy and Quantum Chemical Calculations. *J. Chem. Phys.* **2004,** *122*, 014313.

15. Meloni, G.; Ferguson, M. J.; Neumark, D. M., Negative Ion Photodetachment Spectroscopy of the Al_3O_2, Al_3O_3, Al_4O_x, Al_5O_x(x = 3–5), Al_6O_5, and Al_7O_5 Clusters. *Phys. Chem. Chem. Phys.* **2003,** *5*, 4073-4079.

16. DeVine, J. A.; Babin, M. C.; Neumark, D. M., Photoelectron Spectra of $Al_2O_2^-$ and $Al_3O_3^-$ via Slow Electron Velocity-Map Imaging. *Faraday Discuss.* **2019,** *217*, 235-255.

17. Archibong, E. F.; St-Amant, A., On the Structure of Al_2O_3 and Photoelectron Spectra of $Al_2O_2^-$ and Al_2O_3. *J. Phys. Chem. A* **1999,** *103*, 1109-1114.

18. van Heijnsbergen, D.; Demyk, K.; Duncan, M. A.; Meijer, G.; von Helden, G., Structure Determination of Gas Phase Aluminum Oxide Clusters. *Phys. Chem. Chem. Phys.* **2003,** *5*, 2515-2519.

19. Stosser, G.; Schnockel, H., The Molecules AlO_2, $Al(O_2)_2$, and $Al(O_2)_3$: Experimental and Quantum-Chemical Investigations on the Oxidation of Aluminum Atoms. *Angew. Chem. Int. Ed. Engl.* **2005,** *44*, 4261-4264.

20. Sierka, M.; Doebler, J.; Sauer, J.; Santambrogio, G.; Bruemmer, M.; Woeste, L.; Janssens, E.; Meijer, G.; Asmis, K. R., Unexpected Structures of Aluminum Oxide Clusters in the Gas Phase. *Angew. Chem. Int. Edit.* **2007,** *46*, 3372-3375.

21. Santambrogio, G.; Janssens, E.; Li, S.; Siebert, T.; Meijer, G.; Asmis, K. R.; Doebler, J.; Sierka, M.; Sauer, J., Identification of Conical Structures in Small Aluminum Oxide Clusters: Infrared Spectroscopy of $(Al_2O_3)_{(1-4)}(AlO)^+$. *J. Am. Chem. Soc.* **2008,** *130*, 15143-15149.

22. Sierka, M.; Döbler, J.; Sauer, J.; Zhai, H.-J.; Wang, L.-S., The $[(Al_2O_3)_2]^-$ Anion Cluster: Electron Localization–Delocalization Isomerism. *ChemPhysChem* **2009,** *10*, 2410-2413.

23. Song, X.; Fagiani, M. R.; Gewinner, S.; Schoellkopf, W.; Asmis, K. R.; Bischoff, F. A.; Berger, F.; Sauer, J., Gas Phase Structures and Charge localization in Small Aluminum Oxide Anions: Infrared Photodissociation Spectroscopy and Electronic Structure Calculations. *J. Chem. Phys.* **2016,** *144*, 244305.

24. Song, X.; Fagiani, M. R.; Gewinner, S.; Schoellkopf, W.; Asmis, K. R.; Bischoff, F. A.; Berger, F.; Sauer, J., Gas-Phase Vibrational Spectroscopy of the Aluminum Oxide Anions $(Al_2O_3)_{(1-6)}AlO_2^-$. *Chemphyschem* **2017,** *18*, 868-872.

25. Debnath, S.; Knorke, H.; Schollkopf, W.; Zhou, S. D.; Asmis, K. R.; Schwarz, H., Experimental Identification of the Active Site in the Heteronuclear Redox Couples

$AlVO_x^{+\cdot}/CO/N_2O$ (x = 3 ,4) by Gas-Phase IR Spectroscopy. *Angew. Chem. Int. Ed.* **2018,** *57*, 7448-7452.

26. Müller, F.; Stuckrath, J. B.; Bischoff, F. A.; Gagliardi, L.; Sauer, J.; Debnath, S.; Jorewitz, M.; Asmis, K. R., Valence and Structure Isomerism of $Al_2FeO_4^+$: Synergy of Spectroscopy and Quantum Chemistry. *J. Am. Chem. Soc.* **2020,** *142*, 18050-18059.
27. Asmis, K. R.; Brümmer, M.; Kaposta, C.; Santambrogio, G.; von Helden, G.; Meijer, G.; Rademann, K.; Wöste, L., Mass-Selected Infrared Photodissociation Spectroscopy of $V_4O_{10}^+$. *Phys. Chem. Chem. Phys.* **2002,** *4*, 1101-1104.
28. Brümmer, M.; Kaposta, C.; Santambrogio, G.; Asmis, K. R., Formation and Photodepletion of Cluster Ion-Messenger Atom Complexes in a Cold Ion Trap: Infrared Spectroscopy of VO^+, VO_2^+, and VO_3^+. *J. Chem. Phys.* **2003,** *119*, 12700-12703.
29. Maeda, S.; Ohno, K.; Morokuma, K., Systematic Exploration of the Mechanism of Chemical Reactions: the Global Reaction Route Mapping (GRRM) Strategy Using the ADDF and AFIR Methods. *Phys. Chem. Chem. Phys.* **2013,** *15*, 3683-3701.
30. Maeda, S.; Taketsugu, T.; Morokuma, K., Exploring Transition State Structures for Intramolecular Pathways by the Artificial Force Induced Reaction Method. *J. Comput. Chem.* **2014,** *35*, 166-173.
31. Maeda, S.; Harabuchi, Y.; Takagi, M.; Taketsugu, T.; Morokuma, K., Artificial Force Induced Reaction (AFIR) Method for Exploring Quantum Chemical Potential Energy Surfaces. *Chem. Rec.* **2016,** *16*, 2232-2248.
32. Goebbert, D. J.; Wende, T.; Bergmann, R.; Meijer, G.; Asmis, K. R., Messenger-Tagging Electrosprayed Ions: Vibrational Spectroscopy of Suberate Dianions. *J. Phys. Chem. A* **2009,** *113*, 5874-5880.

33. Goebbert, D. J.; Meijer, G.; Asmis, K. R., 10K Ring Electrode Trap - Tandem Mass Spectrometer for Infrared Spectroscopy of Mass Selected Ions. *AIP Conf. Proc.* **2009,** *1104*, 22-29.

34. Wieland, S.; Sandy, G.; Heinz, J.; Alexander, P.; Gert von, H.; Hans, P. B.; Alan, M. M. T. In *The new IR and THz FEL facility at the Fritz Haber Institute in Berlin*, Proc.SPIE, 2015.

35. Heine, N.; Asmis, K. R., Cryogenic Ion Trap Vibrational Spectroscopy of Hydrogen-Bonded Clusters Relevant to Atmospheric Chemistry. *Int. Rev. Phys. Chem.* **2015,** *34*, 1-34.

36. Heine, N.; Asmis, K. R., Cryogenic Ion Trap Vibrational Spectroscopy of Hydrogen-Bonded Clusters Relevant to Atmospheric Chemistry. *Int. Rev. Phys. Chem.* **2016,** *35*, 507-507.

37. Maeda, S.; Harabuchi, Y.; Takagi, M.; Saita, K.; Suzuki, K.; Ichino, T.; Sumiya, Y.; Sugiyama, K.; Ono, Y., Implementation and Performance of the Artificial Force Induced Reaction Method in the GRRM17 Program. *J. Comput. Chem.* **2018,** *39*, 233-251.

38. Grrm. S. Maeda, Y. H., Y. Sumiya, M. Takagi, K. Suzuki, M. Hatanaka, Y. Osada, T. Taketsugu, K. Morokuma, K. Ohno, GRRM17. *Http://Iqce.Jp/GRRM/Index_e.Shtml.*

39. Debnath, S.; Song, X.; Fagiani, M. R.; Weichman, M. L.; Gao, M.; Maeda, S.; Taketsugu, T.; Schöllkopf, W.; Lyalin, A.; Neumark, D. M.; Asmis, K. R., CO_2 Adsorption on $Ti_3O_6^-$: A Novel Carbonate Binding Motif. *J. Phys. Chem. C* **2019,** *123*, 8439-8446.

40. Song, X.; Fagiani, M. R.; Debnath, S.; Gao, M.; Maeda, S.; Taketsugu, T.; Gewinner, S.; Schöllkopf, W.; Asmis, K. R.; Lyalin, A., Excess Charge Driven Dissociative Hydrogen Adsorption on $Ti_2O_4^-$. *Phys. Chem. Chem. Phys.* **2017,** *19*, 23154-23161.

41. Gao, M.; Lyalin, A.; Maeda, S.; Taketsugu, T., Application of Automated Reaction Path Search Methods to a Systematic Search of Single-Bond Activation Pathways Catalyzed by

Small Metal Clusters: A Case Study on H–H Activation by Gold. *J. Chem. Theory Comput.* **2014,** *10*, 1623-1630.

42. TURBOMOLE V7.0-7.5 2020, a Development of University of Karlsruhe and Forschungszentrum Karlsruhe GmbH, 1989-2007, TURBOMOLE GmbH, since 2007; Available from Https://Www.Turbomole.Org.
43. Balasubramani, S. G.; Chen, G. P.; Coriani, S.; Diedenhofen, M.; Frank, M. S.; Franzke, Y. J.; Furche, F.; Grotjahn, R.; Harding, M. E.; Hättig, C.; Hellweg, A.; Helmich-Paris, B.; Holzer, C.; Huniar, U.; Kaupp, M.; Khah, A. M.; Khani, S. K.; Müller, T.; Mack, F.; Nguyen, B. D.; Parker, S. M.; Perlt, E.; Rappoport, D.; Reiter, K.; Roy, S.; Rückert, M.; Schmitz, G.; Sierka, M.; Tapavicza, E.; Tew, D. P.; Wüllen, C. v.; Voora, V. K.; Weigend, F.; Wodyński, A.; Yu, J. M., TURBOMOLE: Modular Program Suite for ab Initio Quantum-Chemical and Condensed-Matter Simulations. *J. Chem. Phys.* **2020,** *152*, 184107.
44. Schäfer, A.; Horn, H.; Ahlrichs, R., Fully Optimized Contracted Gaussian Basis Sets for Atoms Li to Kr. *J. Chem. Phys.* **1992,** *97*, 2571-2577.
45. Perdew, J. P., Density-Functional Approximation for the Correlation Energy of the Inhomogeneous Electron Gas. *Phys. Rev. B* **1986,** *33*, 8822-8824.
46. Becke, A. D., Density-Functional Exchange-Energy Approximation with Correct Asymptotic Behavior. *Phys. Rev. A* **1988,** *38*, 3098-3100.
47. Eichkorn, K.; Weigend, F.; Treutler, O.; Ahlrichs, R., Auxiliary Basis Sets for Main Row Atoms and Transition Metals and Their Use to Approximate Coulomb Potentials. *Theor. Chem. Acc.* **1997,** *97*, 119-124.
48. Becke, A. D., Density-Functional Thermochemistry. 3. The Role of Exact Exchange. *J. Chem. Phys.* **1993,** *98*, 5648-5652.

49. Lee, C. T.; Yang, W. T.; Parr, R. G., Development of the Colle-Salvetti Correlation-Energy Formula Into a Functional of the Electron-Density. *Phys. Rev. B* **1988,** *37*, 785-789.

50. Weigend, F.; Häser, M.; Patzelt, H.; Ahlrichs, R., RI-MP2: Optimized Auxiliary Basis Sets and Demonstration of Efficiency. *Chem. Phys. Lett.* **1998,** *294*, 143-152.

51. Weigend, F.; Ahlrichs, R., Balanced Basis Sets of Split Valence, Triple Zeta Valence and Quadruple Zeta Valence Quality for H to Rn: Design and Assessment of Accuracy. *Phys. Chem. Chem. Phys.* **2005,** *7*, 3297-3305.

52. Gaussian 16, Revision C.01, M. J. Frisch, G. W. Trucks, H. B. Schlegel, G. E. Scuseria, M. A. Robb, J. R. Cheeseman, G. Scalmani, V. Barone, G. A. Petersson, H. Nakatsuji, X. Li, M. Caricato, A. V. Marenich, J. Bloino, B. G. Janesko, R. Gomperts, B. Mennucci, H. P. Hratchian, J. V. Ortiz, A. F. Izmaylov, J. L. Sonnenberg, D. Williams-Young, F. Ding, F. Lipparini, F. Egidi, J. Goings, B. Peng, A. Petrone, T. Henderson, D. Ranasinghe, V. G. Zakrzewski, J. Gao, N. Rega, G. Zheng, W. Liang, M. Hada, M. Ehara, K. Toyota, R. Fukuda, J. Hasegawa, M. Ishida, T. Nakajima, Y. Honda, O. Kitao, H. Nakai, T. Vreven, K. Throssell, J. A. Montgomery, Jr., J. E. Peralta, F. Ogliaro, M. J. Bearpark, J. J. Heyd, E. N. Brothers, K. N. Kudin, V. N. Staroverov, T. A. Keith, R. Kobayashi, J. Normand, K. Raghavachari, A. P. Rendell, J. C. Burant, S. S. Iyengar, J. Tomasi, M. Cossi, J. M. Millam, M. Klene, C. Adamo, R. Cammi, J. W. Ochterski, R. L. Martin, K. Morokuma, O. Farkas, J. B. Foresman, and D. J. Fox, Gaussian, Inc., Wallingford CT, 2019.

53. Kempkes, L. J. M.; Martens, J.; Berden, G.; Houthuijs, K. J.; Oomens, J., Investigation of the Position of the Radical in z(3)-ions Resulting From Electron Transfer Dissociation Using Infrared Ion Spectroscopy. *Faraday Discuss.* **2019,** *217*, 434-452.

54. Jiang, W.; DeYonker, N. J.; Wilson, A. K. Multireference Character for 3d Transition-Metal-Containing Molecules. *J. Chem. Theory Comput.* **2012**, *8*, 460-468.

55. Andersson, K.; Malmqvist, P. A.; Roos, B. O.; Sadlej, A. J.; Wolinski, K. Second-Order Perturbation Theory with a CASSCF Reference Function. *J. Phys. Chem.* **1990**, *94*, 5483-5488.

56. Werner, H. J.; Knowles, P. J. An Efficient Internally Contracted Multiconfiguration–Reference Configuration Interaction Method. *J. Chem. Phys.* **1988**, *89*, 5803-5814.

57. Feyel, S.; Döbler, J.; Hoeckendorf, R.; Beyer, M. K.; Sauer, J.; Schwarz, H. Activation of Methane by Oligomeric $(Al_2O_3)_x^+$ (x = 3, 4, 5): The Role of Oxygen-Centered Radicals in Thermal Hydrogen-Atom Abstraction. *Angew. Chem. Int. Edit.* **2008**, *47*, 1946-1950.

58. Lau, J. T.; Rittmann, J.; Zamudio-Bayer, V.; Vogel, M.; Hirsch, K.; Klar, P.; Lofink, F.; Möller, T.; v. Issendorff, B., Size Dependence of $L_{2,3}$ Branching Ratio and 2*p* Core-Hole Screening in X-Ray Absorption of Metal Clusters. *Phys. Rev. Lett.* **2008,** *101,* 153401.

Table 1. O/Al ratio, average coordination numbers (CN), number of terminal oxygen radical anions ($O_t^{-\bullet}$) and peroxide (O_2^{2-}) units as well as Ni oxidation state (OS) for all low−energy isomers.

Isomer	O/Al ratio	Average CN		Ni CN	$O^{-\bullet}$	O_2^{2-}	Ni OS
		O^{av}	Al^{av}				
A−1	1.67	2.2	3	2	0	0	+2
B−1	1.6	2.25	3.2	2	0	0	+2
C−1	1.57	2.36	3.29	3	0	0	+2
D−1	2	2.02	3	3	1	0	+3
D−2	2	2.33	3.33	2	0	1	+2
E−1	1.8	2.11	3.2	3	1	0	+3
F−1	1.71	2.33	3.29	3	0	1	+2
F−2	1.71	2.47	3.57	3	0	1	+2
armorphous alumina	1.53	2−3	4−5				
thin film	1.3	3.0	3.9				
−alumina	1.5	4	6				

Table 2. Experimental and calculated scaled harmonic vibrational frequencies (in cm^{-1}) of different oxygen species in $(NiO_2)(Al_2O_3)_n(AlO)^+$ with n = 1−3 and the related Al–$O_t^{\bullet}$/O-O Bond length (pm).

Species	Cluster	Isomer	Exp.	B3LYP	Al−O/O−O Bond Length
Terminal Al–$O_t^{\bullet}$	n = 1	**D−1**	912	906	172
	n = 2	**E−1**	933	920	172
Peroxide	n = 1	**D−2**	912	895	155
	n = 3	**F−1**	908	911	147
	n = 3	**F−2**	908	864	152

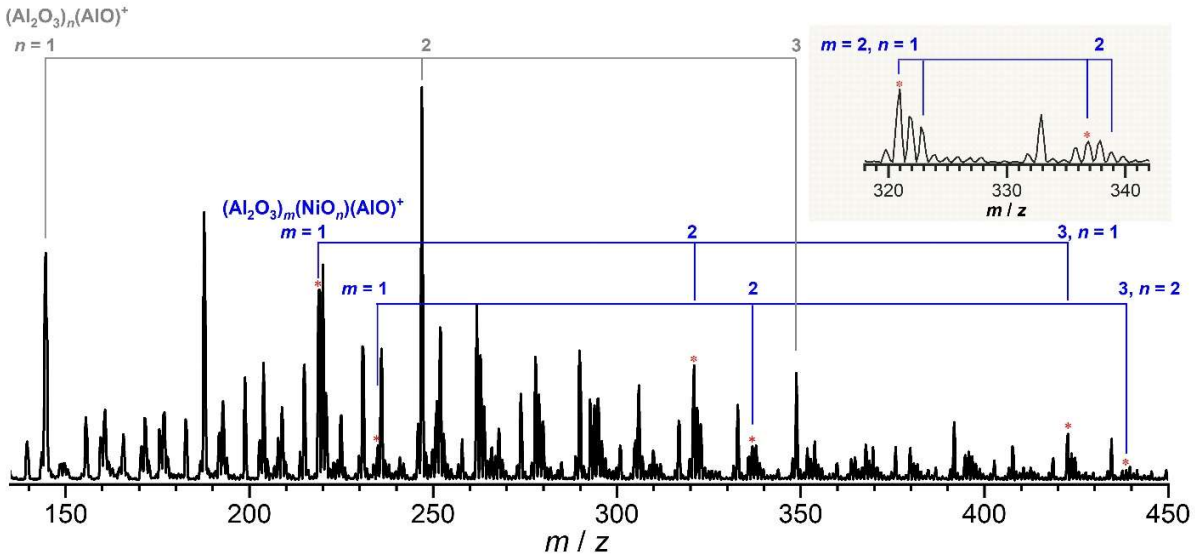

Figure 1. Quadrupole mass spectrum of the cations produced by laser ablation of an Al/Ni rod in the presence of 1% O_2 seeded in He. The dominant mass progressions are labeled.

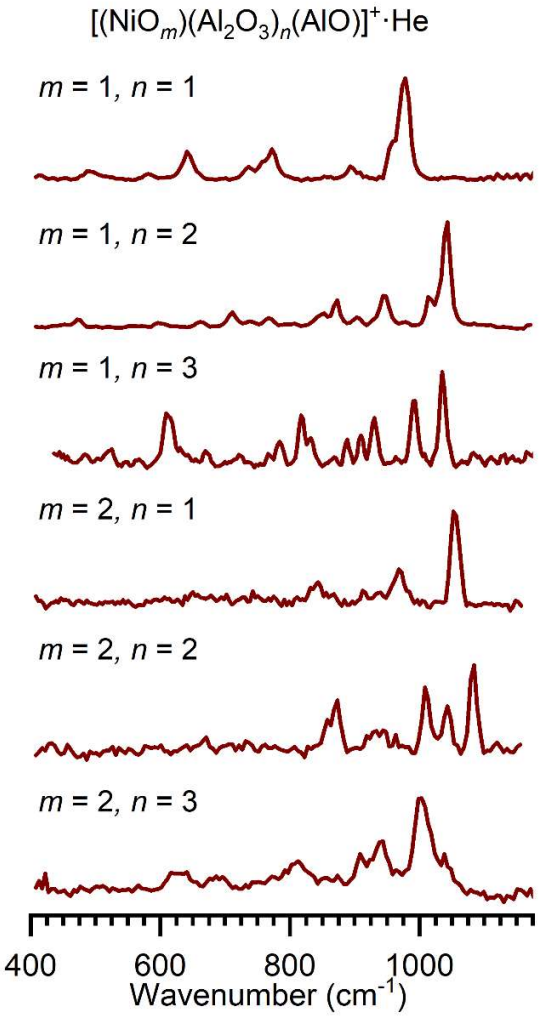

Figure 2. IRPD spectra of He−tagged $(NiO_m)(Al_2O_3)_n(AlO)^+$ cations (m = 1−2, n = 1−3) in the spectral region from 400 to 1175 cm^{-1} measured at an ion trap temperature of 10 K. The vertical scale for each figure is independent.

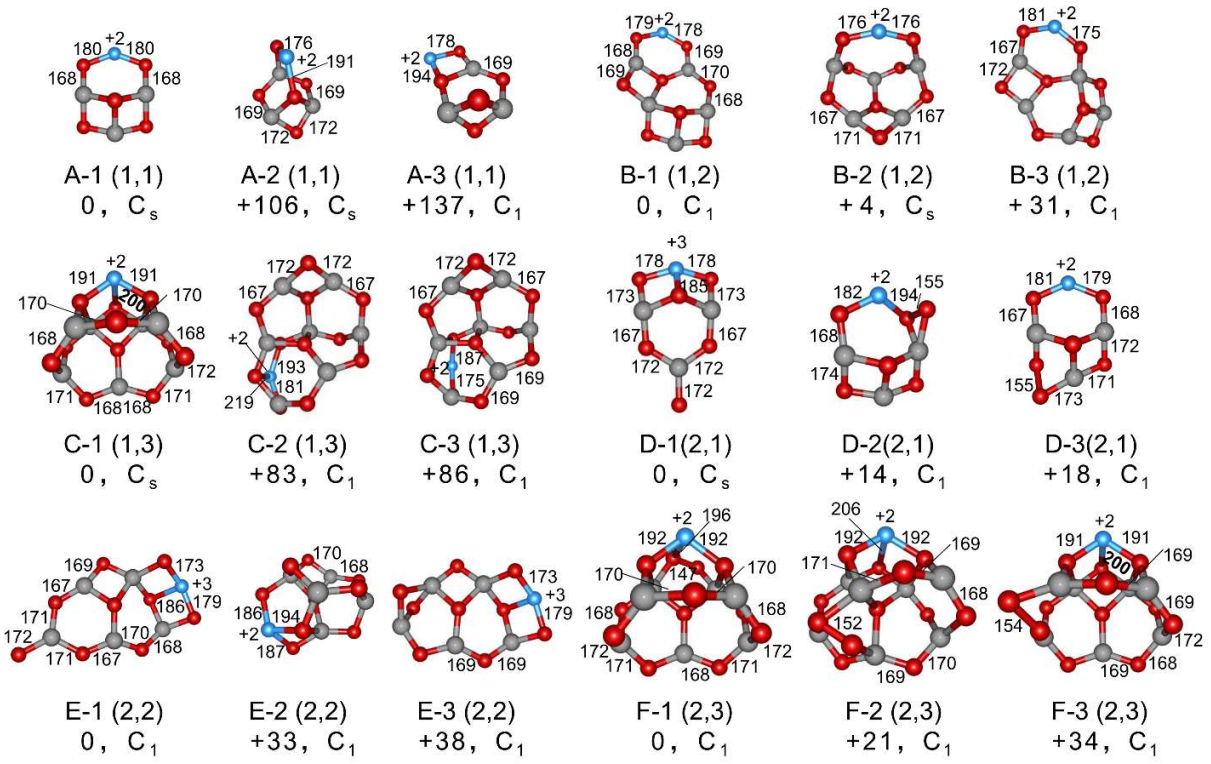

Figure 3. B3LYP/def2−tzvp minimum−energy structures of low energy isomers of $(NiO_m)(Al_2O_3)_n(AlO)^+$ cations with m = 1−2 and n = 1−3 (color code: blue, Ni; gray, Al; red, O). Only electronic triplet states are considered. The number of m and n are denoted as (m, n) below each structure along with the zero−point vibration−corrected energies (ΔH_{0K}) with respect to the related ground state clusters (kJ mol^{-1}), and symmetry of each cluster. Bond lengths for Ni−O bonds, Al−$O_t^{\bullet}$ bonds, peroxide bonds, and bonds involved in the highest frequency vibration are listed in units of pm. The oxidation state of each Ni atom is listed next to the atom in each structure.

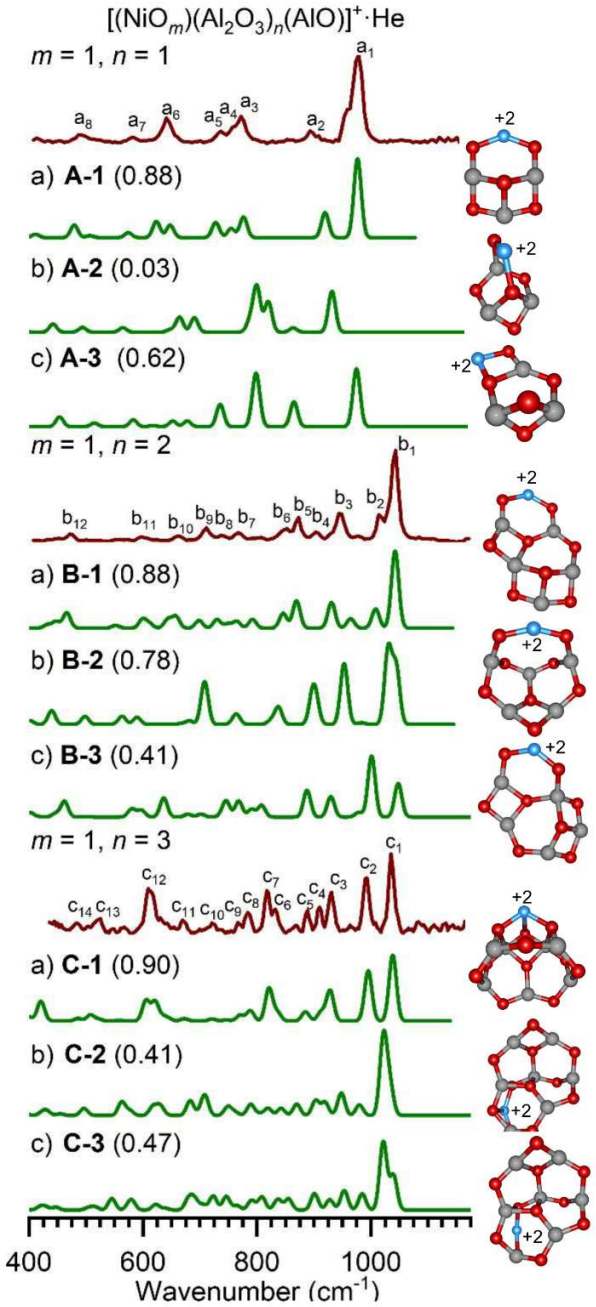

Figure 4. Experimental IRPD spectra (dark red) of He-tagged (NiO)(Al$_2$O$_3$)$_n$(AlO)$^+$ cations with n = 1−3 and simulated IR spectra (green) of low−energy isomers (without He). ZPE-corrected energies ΔH_{0K} are given in kJ mol^{-1}. The cosine similarity score is shown in parentheses. See **Table S1** for the band positions and assignments.

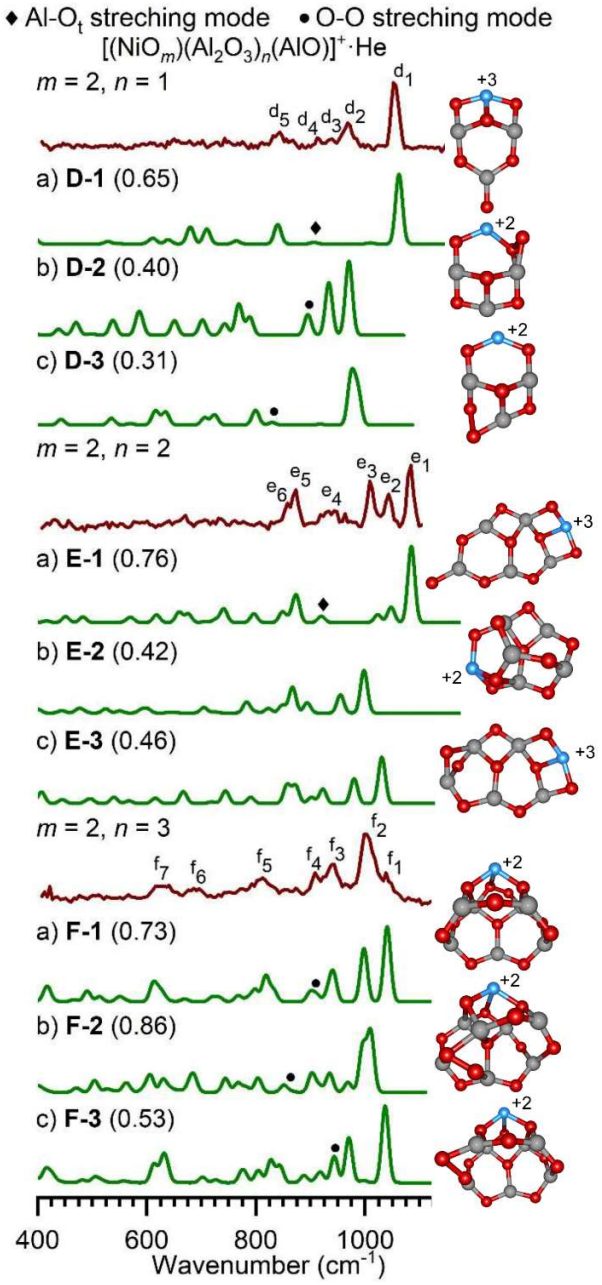

Figure 5. Experimental IRPD spectra (dark red) of He-tagged $(NiO_2)(Al_2O_3)_n(AlO)^+$ cations with n = 1−3 and simulated IR spectra (green) of low−energy isomers (without He). ZPE-corrected energies ΔH_{0K} are given in kJ mol^{-1}. The cosine similarity score is shown in parentheses. See **Table S1** for the band positions and assignments.

TOC

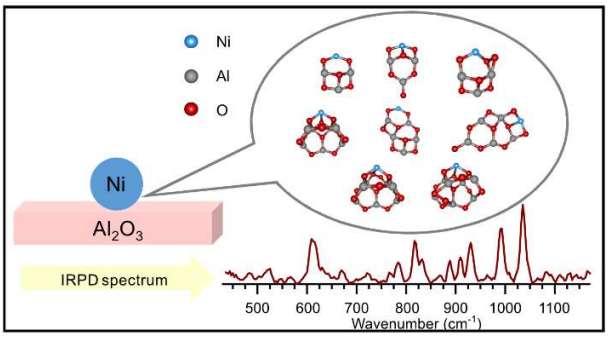
Ni
Al
O
Ni
Al_2O_3
IRPD spectrum
500
600
700
800
900
1000
1100
Wavenumber (cm^{-1})